JPhys Photonics

PURPOSE-LED PUBLISHING™

PAPER • OPEN ACCESS

Thermo-optical properties of α-MoO_3 thin films in the mid-infrared and phonon frequency shift

To cite this article: Alessandro Bile *et al* 2025 *J. Phys. Photonics* **7** 025015

Journal of Physics: Photonics

PAPER

Thermo-optical properties of α-MoO_3 thin films in the mid-infrared and phonon frequency shift

Alessandro Bile[1], **Daniele Ceneda**[1], **Marco Centini**[1,*], **Federico Vittorio Lupo**[2], **Dominique Persano Adorno**[3], **Roberto Macaluso**[2], **Koray Aydin**[4] and **Maria Cristina Larciprete**[1]

[1] Department of Basic and Applied Sciences, Sapienza University of Rome, Rome 00161, Italy
[2] Department of Engineering, University of Palermo, Palermo 90128, Italy
[3] Department of Physics and Chemistry 'E. Segré', University of Palermo, Palermo 90128, Italy
[4] Department of Electrical and Computer Engineering, Northwestern University, Evanston, IL 60208, United States of America
[*] Author to whom any correspondence should be addressed.

E-mail: marco.centini@uniroma1.it

Keywords: MoO_3, optical properties, thermo-optical constants, pulsed laser deposition

OPEN ACCESS

RECEIVED
30 December 2024

REVISED
25 February 2025

ACCEPTED FOR PUBLICATION
4 March 2025

PUBLISHED
14 March 2025

Abstract

We investigate the mid-infrared thermo-optical properties of polycrystalline alpha-phase molybdenum trioxide (α-MoO_3) thin films grown on fused silica substrates via pulsed laser deposition (PLD) at 500 °C. By analyzing temperature-dependent reflection spectra, we determine stable and uniquely defined MoO_3 thermo-optical constants, dn/dT and dk/dT, over a 20 °C–250 °C temperature range. Unlike films grown using other deposition techniques at room temperature and subsequently annealed, our results demonstrate that PLD enables the fabrication of reliable and thermally stable MoO_3 thin films, making them highly suitable for infrared applications, such as filters, polarizers, and sensors.

1. Introduction

The renewed interest in mid-infrared (mid-IR) photonics is driven by wide-ranging applications, including sensitive biosensing [1], control of radiative heat transfer [2], coherent thermal emission [3], and subwavelength radiation control through the excitation of surface phonon polaritons (SPhPs) [4]. Among the materials suitable for such mid-IR applications, single-phase alpha-molybdenum trioxide (α-MoO_3) stands out due to its pronounced optical anisotropy. As a van der Waals (vdW) crystal, α-MoO_3 features atomic planes linked by vdW bonds, making it highly suitable for exfoliation and enabling electronic and ionic conductivity [5].

Similar to other polar dielectric materials, MoO_3 can support the excitation of SPhPs, quasi-particles that emerge from the coupling between phonons (lattice vibrations in a solid material) and photons (light quanta). Remarkably, α-MoO_3 exhibits hyperbolic and biaxial behavior, enabling the formation of SPhPs across three distinct wavelength bands along its orthogonal crystallographic directions [6]. Additionally, MoO_3 demonstrates chromogenic properties [7], such as thermochromism [8, 9], photochromism [10], and electrochromism [11, 12], further expanding its feasibility for potential mid-IR application. Despite these promising structural and optical characteristics, the development of IR photonic devices based on α-MoO_3 is hindered by the difficulty in producing large-area, stable and high-quality single-phase MoO_3 thin films. Optical quality and thermal stability of MoO_3 films are significantly influenced by the synthesis methods employed [13]. Deposition methods based on evaporation often yield MoO_3 films with irregular morphology comprised of micron-sized small domains [14].

Additionally, the films typically undergo a color transition from transparent white to bluish as temperature increases from room temperature to 300 °C [15] accompanied by hysteretic behavior during heating and cooling cycles [16]. This irreversibility strongly impacts the potential usage of this material for applications requiring stable and repeatable control of the optical properties. More in detail, previous studies (limited in the visible and near IR ranges) reveal a non-reversibility of the thermally induced optical properties of MoO_3 films. For instance, thermal treatments in argon of MoO_3 thin films were investigated

and found to have an influence on their thermochromic response, for annealing temperatures in the range 100 °C–225 °C [17]. Specifically, annealing in air at 450 °C produces polycrystalline colorless films where α-MoO_3 is the predominant phase. Another consequence of annealing MoO_3 films in an argon atmosphere is a significant narrowing of their forbidden band gap energy.

The effect of annealing temperature on transmittance properties was investigated in [18] from 400 nm thick MoO_3 thin films where temperature-dependent Raman spectroscopy in MoO_3 submicron rods highlights a phase transformation in the 675–690 K temperature range from the hexagonal phase to the orthorhombic phase [19]. More interestingly, in [20] thermo-optical properties (e.g. refractive index and extinction coefficient versus temperature) and coefficients (e.g. dn/dT and dk/dT) are reported for thermally evaporated MoO_3 thin films using ellipsometry measurements versus temperature in the visible range. The values of thermo-optical coefficients dn/dT and dk/dT over the temperature range 295–460 K have been retrieved in the visible and near-infrared part of the spectral range (0.2–2.4 μm). However, being these films synthesized via thermal deposition at room temperature, their parameters are not uniquely defined across the investigated temperature range, as heating induces structural changes and effectively acts as an annealing process. Moreover, hysteresis effects are reported during heating/cooling cycles, even for annealed samples in vacuum and under oxygen background gas [20]. To investigate the temperature-dependent controllability of the optical properties of α-phase MoO_3 films, a more reliable and repeatable analysis must be conducted on well-crystallized α-phase MoO_3 samples. Among the different deposition techniques to synthesize MoO_3 thin-films, including spray pyrolysis [21], thermal evaporation [20], and plasma assisted sublimation and thermal evaporation [22], Pulsed laser deposition (PLD) [23, 24] allows tailoring the deposition parameters (substrate temperature, oxygen partial pressure) for the fabrication of stable MoO_3 thin films of the desired crystallographic phase and stochiometry without further post-growth annealing steps. Typical deposition temperature for obtaining α-MoO_3 films are in the range between 300 °C and 600 °C [23–27]. Interestingly, Ramana *et al* [28], have reported on α-MoO_3 films deposited by PLD at room temperature. Films crystallization to the α-phase of MoO_3 can be obtained also by a post-growth annealing process at temperatures ranging from 300 °C to 600 °C [26, 29–31]. This means that, according to most of the published works, any study on MoO_3 for IR photonic and polaritonic applications must be conducted on α-MoO_3 thin films deposited or annealed at temperatures ranging between 300 °C and 600 °C.

In this paper, we investigated the thermo-optical properties of α-MoO_3 films fabricated at 500 °C using PLD [23, 24]. We focus our study on temperature-dependent optical characteristics in the 8–12 μm wavelength range. The PLD-grown MoO_3 sample is measured to exhibit a reversible thermal response range (20 °C–250 °C), indicating that despite multiple heating and cooling cycles, the material consistently returns to its initial state without experiencing permanent changes in its crystalline or optical properties. Such reversible behavior is advantageous for applications requiring stability and reproducibility in optical performances. Measured reflectance spectra is used to retrieve a temperature-dependent refractive index and thermo-optical coefficients. Our findings suggest that MoO_3 films fabricated by PLD can be effectively employed in the design of thermally tunable light modulation devices for infrared photonics and thermal radiation management [25, 26], ensuring a predictable and controllable response with temperature variations.

2. Sample fabrication

2200 nm-thick MoO_3 film was deposited onto a fused silica substrate using PLD at 500 °C and 0.1 mbar of oxygen pressure. The employed PLD system utilizes a Q-switched tripled Nd:YAG laser (Quantel mod. YG78C20, $\lambda = 355$ nm), which produces 6 nm-wide pulses with an energy of 80 mJ per pulse [26]. The energy density was kept at 1.2 J cm^{-2} with a repetition rate of 4 Hz. Film deposition was carried out by using a 99.9% pure MoO_3 target (1 inch diameter, 0.25 inch thickness). Prior to deposition, the substrate was cleaned in an ultrasonic bath with acetone, then rinsed with isopropanol, and dried with compressed air.

3. Results and discussion

IR reflectance spectra were measured using a Bruker FT-IR Invenio-R interferometer, equipped with a glow-bar radiation source and a detector based on deuterated triglycine sulfate pyroelectric detector. Each measurement is characterized by the acquisition of 64 interferograms, a sample area of 3 × 3 mm^2, and a spectral resolution of 1 cm^{-1}. The FT-IR system is equipped with a variable angle reflection stage, the incidence angle was fixed at $\theta = 15°$. The instrument operates in the spectral region between 400 and 8000 cm^{-1}. The input light polarization can be varied using a motorized wide-range holographic grid polarizer. In our experiments, the polarization angle was fixed at $\theta = 0°$ (p-polarized), and the material's response was investigated at different temperatures: $T0 = 20$ °C, $T100 = 100$ °C, $T200 = 200$ °C,

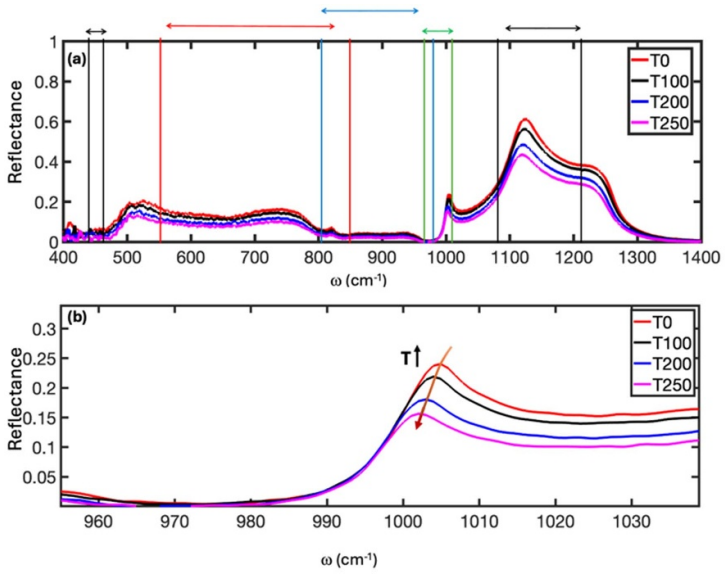

Figure 1. (a) Temperature-dependent reflectance FT-IR spectra measured at $\theta = 15°$ incidence angle and p-polarization from an α-MoO_3 film, grown at 500 °C on fused silica substrate using pulsed laser deposition. The edges of the Restrstrahlen bands are reported in blue for *x*-RB, in red for y-RB, in green for z-RB while black arrows highlight the SiO_2 substrate-RBs. (b) Details of temperature tuning of the reflection peak at 1005 cm^{-1} are reported. By increasing the temperature up to 250 °C it is possible to shift the phonon frequency by 4 cm^{-1}.

$T250 = 250$ °C. The investigated temperature range is limited by the specifications of the heater used. Several spectra have been acquired both in heating and cooling modes highlighting the high reversibility of the process and the temperature stability of the sample.

Measured reflectance spectra of MoO_3 thin films at different temperatures is shown in figure 1. At quasi-normal incidence, the polycrystalline MoO_3 film exhibits three Reststrahlen bands (RBs) associated with single crystal α-MoO_3, thus the anisotropy of the sample is negligible. Specifically, the *x*-RB (blue bar) is in the frequency range between 820 and 972 cm^{-1}, the *y*-RB (red bars) is in the range between 545 and 851 cm^{-1} and the *z*-RB (green bars) located in the region between 962 and 1010 cm^{-1}, partially overlapping the fused silica RB (black bars) which extend from 1070–1240 cm^{-1}.

To investigate the temperature-dependent optical properties of MoO_3 polycrystalline film, we employed a theoretical model assuming that the film behaves as an isotropic and homogenous material with an average optical thickness of 2.2 μm, as established in our previous work [26]. Here, we focus on the frequency range between 950 and 1300 cm^{-1}, where thermal effects notably affect the reflection spectra. Indeed, from figure 1 we note that temperature dependent spectra show interesting features in this range. For example the overlap of two α-MoO_3 RBs (along x- and z- crystal axis) results in a temperature tunable reflection peak between 1000 and 1005 cm^{-1}. As shown by reflectance measurements (figure 1(b)), this peak is strongly tunable with temperature. Specifically, at 20 °C, the peak is characterized by $\omega_{max} = 1005$ cm^{-1} and a full width at half maximum $\Delta\omega = 17$ cm^{-1}, thus giving a quality factor $Q = \omega_{max}/\Delta\omega = 59$. When the temperature is increased up to $T = 250$ °C, the peak frequency shifts to $\omega_{max} = 1001$ cm^{-1} while $\Delta\omega = 20$ cm^{-1}, thus resulting in a $Q \sim 50$. We also note that the contribution of the transverse optical phonon resonance of the SiO_2 substrate is responsible for a temperature tunable reflectance band in the 1100–1200 cm^{-1} range.

First, we measured the reflectance spectrum of bare SiO_2 substrate under various temperature conditions to quantify the substrate's contributions to overall temperature-dependent reflection spectra. Using these experimental results, we extracted the temperature-dependent dielectric constant at different temperatures (room temperature, 100 °C, 200 °C and 250 °C) by fitting the corresponding measured spectra. The retrieved dielectric constants were subsequently incorporated into a 4 × 4 transfer matrix method code [32, 33]. The experimental spectra and fit curves for SiO_2 are reported in figure 2. The SiO_2 electric permittivity has been modeled by a single Lorentz oscillator model:

$$\varepsilon_{SiO_2}(\omega) = \varepsilon_\infty + \frac{S_0\omega_0^2}{\omega_0^2 - i\gamma_0\omega - \omega^2} \quad (1)$$

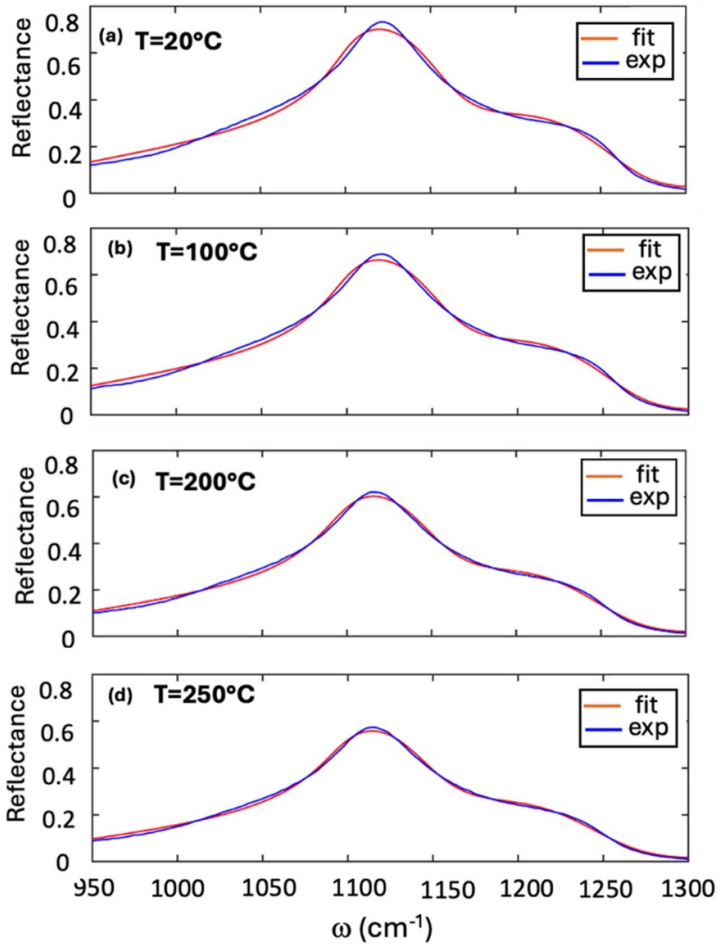

Figure 2. Detail of SiO_2 substrate reflectance FT-IR spectra measured at 15° incidence angle and p-polarization angle (blue curves) along with the corresponding theoretical fit (red curves) for the four investigated temperatures (20 °C, 100 °C, 200 °C, 250 °C).

Table 1. Fitted Lorentz oscillator parameters for the SiO_2 substrate.

T [°C]	S_0	ω_0 [cm^{-1}]	γ_0 [cm^{-1}]	ε_∞	RMS
20	1.27	1192	111.54	4.32	0.016
100	0.95	1190	113.36	3.86	0.013
200	0.93	1186	118.06	3.02	0.010
250	0.82	1184	121.69	2.84	0.008

where ω_o is the phonon frequency, S_o is the oscillator strength, γ_o is the damping coefficient, and ε_∞, the dielectric constant at the high-frequency limit. The results of the fitted parameters for SiO_2 with the associated RMS are listed in table 1.

While SiO_2 dielectric constant in the investigated frequency range could be described by one Lorentz oscillator, the optical response of MoO_3 is mostly driven by three different oscillators representing the three optical phonons along the main crystallographic directions. Typically, in the MoO_3 single crystal the three phonon bands along the three different crystal axis produce an anisotropic behavior and the reflectance spectra are strongly dependent on the polarization and direction of the incident beam. However, from our previous work [26] we have shown that PLD sputtered MoO_3 is polycrystalline, with randomly oriented domains. Thus the response of the three phonon bands, related to x-, y- and z- axis respectively, appears equally mixed for all the directions and polarizations of the incident field, resulting in a isotropic response in the mid-IR range ($\varepsilon_{xx} = \varepsilon_{yy} = \varepsilon_{zz} = \varepsilon$). Furthermore, the lower frequency phonon (at 550 cm^{-1}) has a minimal impact on the overall frequency-dependent electric permittivity in the investigated wavelength range (950–1300 cm^{-1}) and its constant contribution can be included in the ε_∞. These considerations enable us to reduce the number of fitting parameters. Consequently, we can utilize a two-oscillator model

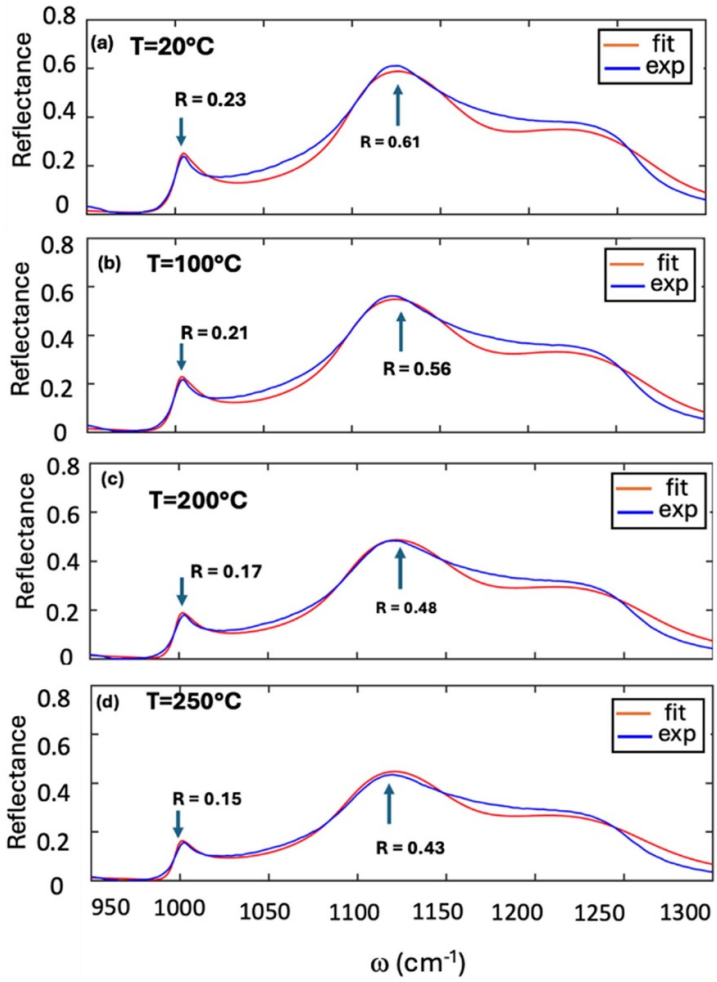

Figure 3. Detail of MoO_3 reflectance FT-IR spectra measured at 15° incidence angle and p-polarization state (blue curves) and the corresponding theoretical fit (red curves) for the four temperatures (20 °C, 100 °C, 200 °C, 250 °C).

Table 2. Fitted Lorentz oscillator parameters for the polycrystalline α-MoO_3 film.

T [°C]	$S_1(S_2)$ [10^{-2}]	$\omega_1(\omega_2)$ [cm^{-1}]	$\gamma_1(\gamma_2)$ [cm^{-1}]	ε_∞	RMS
20	17 (2.2)	846 (1004)	15.4 (3.2)	2.32	0.030
100	17 (1.9)	840 (999)	16.0 (4.6)	2.06	0.027
200	16 (1.5)	831 (998)	16.5 (5.7)	1.96	0.024
250	10 (1.3)	830 (997)	16.9 (6.4)	1.83	0.020

rather than a three-oscillator one:

$$\varepsilon_{MoO_3}(\omega) = \varepsilon_\infty + \sum_{i=1}^{2} \frac{S_i \omega_i^2}{\omega_i^2 - i\gamma_i \omega - \omega^2} \tag{2}$$

where the resonance frequencies ω_i, oscillator strengths S_i, damping coefficients γ_i in equation (1), for $i = 1$, 2, respectively, and ε_∞, are determined as fitting parameters by minimizing the RMS deviation between the calculated and measured reflection signal. The fitting procedure, similar to the one performed for the substrate, has been applied to the experimental spectra recorded at 15° incidence angle for temperatures $T0 = 20$ °C, $T100 = 100$ °C, $T200 = 200$ °C, $T250 = 250$ °C. Reflectance spectra have been calculated for each temperature by considering the proper substrate (SiO_2) dielectric constant as reported in table 1. The obtained results, shown in figure 3, display very good agreement with experiments while the maximum RMS obtained in the fitting procedure is 0.030. The fitting parameters along with the associated RMS are listed in table 2.

Finally, we report in figure 3 the measured FT-IR spectra for each temperature with the corresponding fitting curve. The reflectance values corresponding to two peaks, at $\omega = 1006$ cm^{-1} and at $\omega = 1120$ cm^{-1} respectively, are also highlighted. Figure 4 reports the optical and thermo-optical properties of the MoO_3

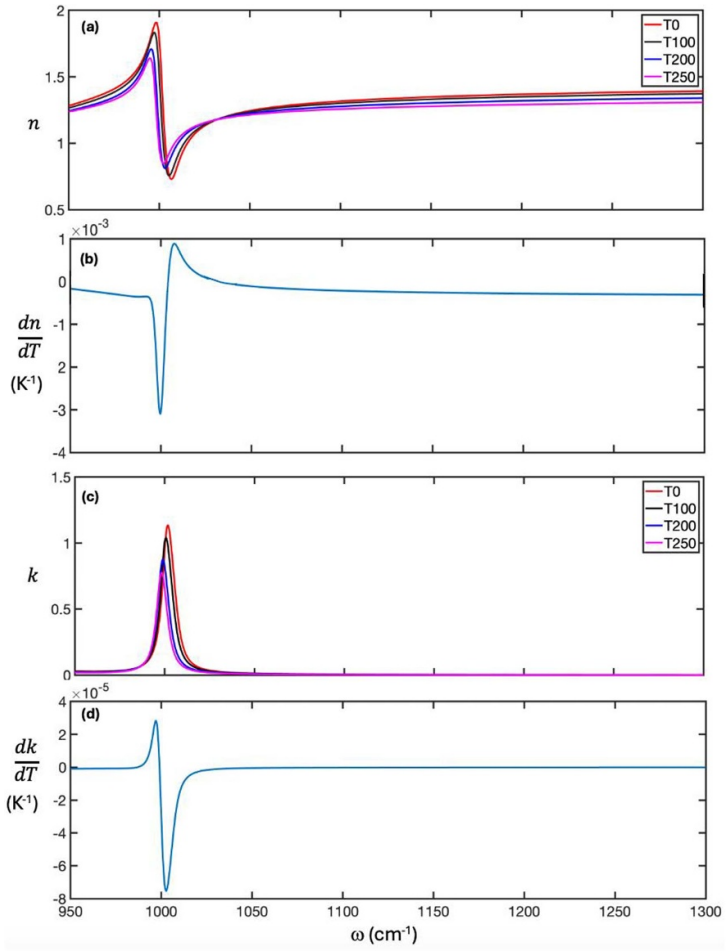

Figure 4. Retrieved optical and thermo-optical properties of the α-MoO_3 film: (a) real part of the refractive index of MoO_3 for each temperature ($T0 = 20\ ^\circ C$, $T100 = 100\ ^\circ C$, $T200 = 200\ ^\circ C$, $T250 = 250\ ^\circ C$); (b) derivative of the real part of the refractive index with respect to the temperature, dn/dT; (c) imaginary part of the refractive index of MoO_3 for each temperature ($T0 = 20\ ^\circ C$, $T100 = 100\ ^\circ C$, $T200 = 200\ ^\circ C$, $T250 = 250\ ^\circ C$); (d) derivative of the imaginary part of the refractive index with respect to the temperature, dk/dT.

film, retrieved from the reflectance measurements versus temperature. From figure 4(a), it can be seen that the MoO_3 refractive index decreases with increasing temperature except for the anomalous dispersion region, where it increases with temperature, corresponding to a positive value of dn/dT, as shown in figure 4(b). As already evidenced by experimental spectral curves, the MoO_3 absorption coefficient k, reported in figure 4(c), shows that there is a phonon shift of about 5 cm^{-1} with increasing temperature.

The thermo-optical coefficients dn/dT and dk/dT were determined by performing a linear fit of the retrieved refractive indices as a function of temperature for each frequency. Figure 5 illustrates the fitting procedure for two relevant frequencies, $\boldsymbol{\omega}_1 = 998\ cm^{-1}$, (figure 5(a), near the MoO_3 phonon frequency) and $\boldsymbol{\omega}_2 = 1094\ cm^{-1}$ (figure 5(b), where MoO_3 is nearly transparent). At these frequencies, the refractive index values at different temperatures are plotted, where the slope of the linear fit represents the dn/dT coefficient. From figure 5 is possible to see that the refractive index decreases with temperature and goes back to its initial value after the cooling process. This shows, unlike MoO_3 films deposited by thermal evaporation [20, 34], a perfect thermal stability of α-MoO_3 films deposited by PLD. This stability could be ascribed to the MoO_3 films crystallization and phase stability achieved during the high temperature growth.

Using this approach, the dn/dT coefficient at resonance ($\omega_1 = 998\ cm^{-1}$) was found to be as high as $(-3.11 \pm 0.04) \times 10^{-3}\ K^{-1}$. Off-resonance, ($\omega_2 = 1094\ cm^{-1}$), the modulus of the coefficient was significantly smaller: $(-1.69 \pm 0.02) \times 10^{-4}\ K^{-1}$. This off-resonance value is comparable to previously reported results in the visible range, where MoO_3 is transparent [9].

Finally, we plot in figure 6 the shift of the reflection peak frequency highlighted in the inset of figure 1 as a function of the temperature. Temperature values have been selected by optimizing the visibility of the shift of the reflectance peak according to the adopted spectral resolution of the FTIR measurements as evidenced by the error bars. A linear regression can be performed as a function of temperature, as reported in figure 6. The almost perfect linear behaviors of the real part of the refractive index (figures 5(a) and (b)) and the

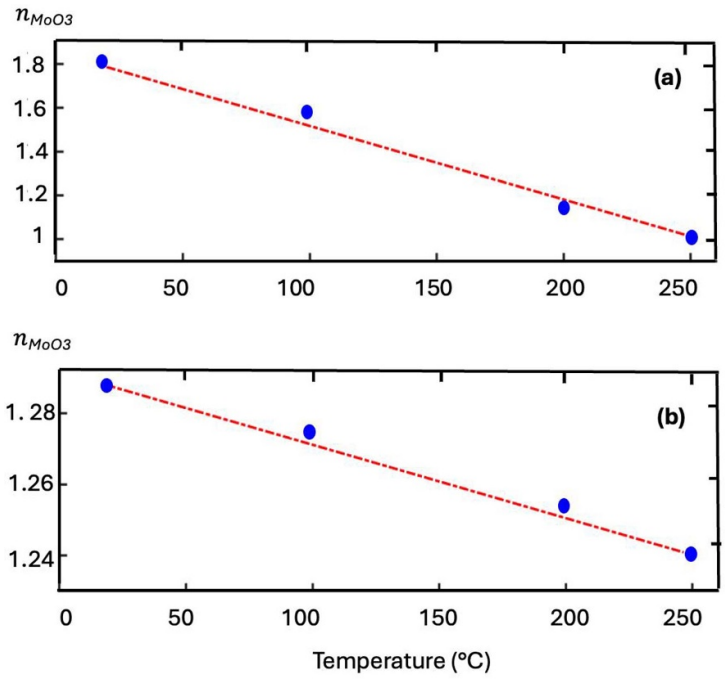

Figure 5. Refractive index values (real part) as a function of temperature measured at (a) $\omega_1 = 998$ cm^{-1} and (b) $\omega_2 = 1094$ cm^{-1} for MoO_3. For each frequency, the thermo-optic coefficient dn/dT of MoO_3 was calculated by fitting the index behavior as a function of the temperature.

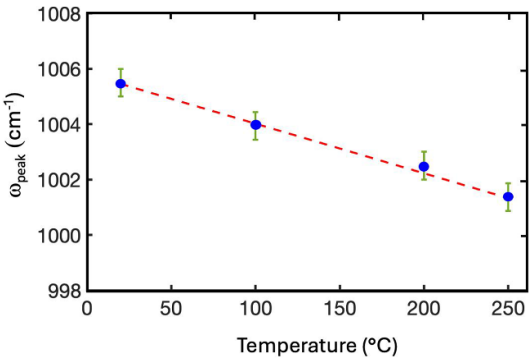

Figure 6. Frequency-shift of the reflection peak (1006 cm^{-1} at room temperature) as a function of the temperature.

linear frequency shift of the reflectance peak in figure 6 confirm the temperature stability of the investigated material with negligible nonlinear and/or irreversible response.

4. Conclusions

We investigated the thermo-optical behavior of α-MoO_3 thin films fabricated by PLD. Using experimentally measured reflectance spectra collected at various temperatures, we developed a fitting model to extract temperature-dependent complex refractive index as well as thermo-optical constants. No evidence of permanent temperature-induced modifications to the optical properties was observed. The stability of the films was further confirmed by the linear dependence of the temperature on the refractive index. Our results evidenced the ability to grow large-area MoO_3 films with a stable alpha crystalline phase and exceptional thermal stability, using PLD at appropriate temperatures. This is in stark contrast to previously reported MoO_3 films deposited at room temperature and subsequently annealed at higher temperatures, which exhibited poor stability. Our findings emphasize the critical role of the deposition technique in the design and development of advanced adaptive, dynamic and stable photonic and optical devices for operations in the infrared region.

Data availability statement

All data that support the findings of this study are included within the article (and any supplementary files).

Acknowledgments

The work was financed by the European Union—Next Generation EU—PNRR M4—C2 -investimento 1.1: Fondo per il Programma Nazionale di Ricerca e Progetti di Rilevante Interesse Nazionale (PRIN)—PRIN 2022 PNRR (Directorial Decree n. 1409–14 September 2022, Project code: P2022X4W28, Title: Mid infrared metasurfaces and metamaterials for microplastic sensing applications, CUP: B53D23028680001). K.A. and M.C.L. acknowledge Accordi Bilaterali Interuniversitari 2022 program from Sapienza University (Prot. AI2620PAR2, Bando Professori Visitatori 2022).

ORCID iDs

Alessandro Bile https://orcid.org/0000-0002-4112-2544
Daniele Ceneda https://orcid.org/0009-0002-4893-6310
Marco Centini https://orcid.org/0000-0003-0625-0054
Federico Vittorio Lupo https://orcid.org/0000-0001-5761-698X
Dominique Persano Adorno https://orcid.org/0000-0001-7655-1114
Roberto Macaluso https://orcid.org/0000-0002-7612-3192
Maria Cristina Larciprete https://orcid.org/0000-0002-7876-628X

References

[1] Rangel G F, de León Martínez L D, Walter L S and Mizaikoff B 2024 Recent advances and trends in mid-infrared chem/bio sensors *TRAC Trends Anal. Chem.* **180** 117916
[2] Liang S, Xu F, Li W, Yang W, Cheng S, Yang H, Chen J, Yi Z and Jiang P 2023 Tunable smart mid infrared thermal control emitter based on phase change material VO2 thin film *Appl. Therm. Eng.* **232** 121074
[3] Sun K, Cai Y, Huang L and Han Z 2024 Ultra-narrowband and rainbow-free mid-infrared thermal emitters enabled by a flat band design in distorted photonic lattices *Nat. Commun.* **15** 4019
[4] Gubbin C R, De Liberato S and Folland T G 2022 Surface phonon polaritons for infrared optoelectronics *J. Appl. Phys.* **131** 030901
[5] Basov D N, Fogler M M and García de Abajo F J 2016 Polaritons in van der Waals materials *Science* **354** 6309
[6] Dereshgi S A, Folland T G, Murthy A A, Song X, Tanriover I, Dravid V P, Caldwell J D and Aydin K 2020 Lithography-free IR polarization converters via orthogonal in-plane phonons in α-MoO_3 flakes *Nat. Commun.* **11** 5771
[7] Vik M and Periyasamy A P 2018 *Chromic Materials: Fundamentals, Measurements, and Applications* 1st edn, ed M Viková (Apple Academic Press) (https://doi.org/10.1201/9781351171007)
[8] Sreelakshmi V R, Anu Kaliani A and Jithin M 2022 Study of thermochromic and photocatalytic properties of MoO_3 thin films *Superlattices Microstruct.* **161** 107096
[9] Dereshgi S A, Larciprete M C, Centini M, Murthy A A, Tang Junqiao K, Vinayak W, Dravid P and Aydin K 2021 Tuning of optical phonons in α-MoO_3–VO_2 multilayers *ACS Appl. Mater. Interfaces* **13** 48981–7
[10] Cruz-San Martín V, Morales-Luna M, García-Tinoco P E, Pérez-González M, Arvizu M A, Crotte-Ledesma H, Ponce-Mosso M and Tomás S A 2018 Chromogenic MoO_3 thin films: thermo-, photo-, and electrochromic response to working pressure variation in rf reactive magnetron sputtering *J. Mater. Sci., Mater. Electron.* **29** 15486–95
[11] Gesheva K A, Ivanova T M and Bodurov G 2012 Transition metal oxide films: technology and "Smart Windows" electrochromic device performance *Prog. Org. Coat.* **74** 635–9
[12] Hsu C-S, Chan C-C, Huang H-T, Peng C-H and Hsu W-C 2008 Electrochromic properties of nanocrystalline MoO_3 thin films *Thin Solid Films* **516** 4839–44
[13] Juan-Arturo A V, Leonel Mendoza-Martínez A, Morales-Luna G and Morales-Luna M 2025 Exploring the optical properties of molybdenum trioxide: approach of theory modeling and depositions techniques *Adv. Phys.* X **10** 2451687
[14] Atuchin V V, Gavrilova T A, Grigorieva T I, Kuratieva N V, Okotrub K A, Pervukhina N V and Surovtsev N V 2011 Sublimation growth and vibrational microspectrometry of α-MoO_3 single crystals *J. Cryst. Growth* **318** 987–90
[15] Pardo A and Torres J 2012 Substrate and annealing temperature effects on the crystallographic and optical properties of MoO_3 thin films prepared by laser assisted evaporation *Thin Solid Films* **520** 1709–17
[16] Kalaev D, Rothschild A and Riess I 2017 Negative differential resistance and hysteresis in Au/MoO_3-d/Au devices *RSC Adv.* **7** 38059
[17] Arvizu M A, Morales-Luna M, Pérez-González M, Campos-Gonzalez E, Zelaya-Angel O and Tomás S A 2017 Influence of thermal annealings in argon on the structural and thermochromic properties of MoO_3 thin films *Int. J. Thermophys.* **38** 51
[18] Moura J V B, Silveira J V, da Silva Filho J G, Souza Filho A G, Luz-Lima C and Freire P T C 2018 Temperature-induced phase transition in h-MoO_3: stability loss mechanism uncovered by Raman spectroscopy and DFT calculations *Vib. Spectrosc.* **98** 98–104
[19] Chithambararaj A and Chandra Bose A 2011 Hydrothermal synthesis of hexagonal and orthorhombic MoO3 nanoparticles *J. Alloys Compd.* **509** 8105–10
[20] Hussain Z 2019 Thermo optical properties and related electronic polarizabilities of MoO_3 thin films using ellipsometry *Am. J. Appl. Sci.* **12** 90–110
[21] Boukhachem A, Kamoun O, Mrabet C, Mannai C, Zouaghi N, Yumak A, Boubaker K and Amlouk M 2015 Structural, optical, vibrational and photoluminescence studies of Sn-doped MoO_3 sprayed thin films *Mater. Res. Bull.* **72** 252–63
[22] Sharma R K and Reddy G B 2014 Effect of substrate temperature on the characteristics of α-MoO_3 hierarchical 3D microspheres prepared by facile PVD process *J. Alloys Compd.* **598** 177–83

[23] Holovský J, Horynova E, Horak L, Ridzonova K, Remes Z, Landova L and Sharma R K 2021 Pulsed laser deposition of high-transparency molybdenum oxide thin films *Vacuum* **194** 110613
[24] Park W-H, Lee G-N and Kim J 2018 Reactive-sputtered transparent MoO_3 film for high-performing infrared Si photoelectric devices *Sens. Actuators* A **271** 251–6
[25] Li Voti R *et al* 2024 Optothermal characterization of vanadium dioxide films by infrared thermography *Int. J. Therm. Sci.* **197** 108832
[26] Larciprete M C *et al* 2024 Large-area polycrystalline α-MoO_3 thin films for IR photonics *J. Phys. D: Appl. Phys.* **57** 135107
[27] Cyril Robinson Azariah J, Ponmudi Selvan T, Samuel Rajasekar M, Sheebha I, Vidhya B and Rajesh S 2018 Pulsed laser deposited molybdenum oxides (MoO_3 & MoO_2) thin films for nanoelectronics device application *2018 4th Int. Conf. on Devices, Circuits and Systems (ICDCS)* (*Coimbatore, India*) pp 42–47
[28] Ramana C V, Atuchin V V, Pokrovsky L D, Becker U and Julien C M 2007 Structure and chemical properties of molybdenum oxide thin films *J Vac. Sci. Technol.* A **25** 1166–71
[29] Santhosh S, Mathankumar M, Selva Chandrasekaran S, Nanda Kumar A K, Murugan P and Subramanian B 2017 Effect of ablation rate on the microstructure and electrochromic properties of pulsed-laser-deposited molybdenum oxide thin films *Langmuir* **33** 19–33
[30] Camacho-López M, Escobar-Alarcón L and Haro-Poniatowski E 2004 Structural transformations in MoOx thin films grown by pulsed laser deposition *Appl. Phys.* A **78** 59–65
[31] Soumya S *et al* 2021 Evolution of fractal dimension in pulsed laser deposited MoO_3 film with ablation time and annealing temperature *Appl. Phys.* A **127** 521
[32] Passler N C and Paarmann A 2017 Generalized 4 × 4 matrix formalism for light propagation in anisotropic stratified media: study of surface phonon polaritons in polar dielectric heterostructures *J. Opt. Soc. Am.* B **34** 2128
[33] Bile A, Centini M, Ceneda D, Sibilia C, Passaseo A, Tasco V and Larciprete M C 2024 Tuning of the Berreman mode of GaN/AlxGa1-xN heterostructures on sapphire: the role of the 2D-electron gas in the mid-infrared *Opt. Mater.* **147** 114708
[34] Hussain Z 2019 Ellipsometric investigations of electronic polarizability and thermo-optic coefficients of Z_xMoO_3 (Z = H+, Li+) bronzes *J. Electron. Mater.* **48** 7427–40